Appropriate cumulative fatigue damage models for fatigue life estimation applied to high-strength steels

Stanislav Seitl[1,2]*, Mohammad S. Al Khazali[1,2], Lucie Malikova[1,2]

[1]*Institute of Physics of Materials, Czech Academy of Sciences, v. v. i., Žižkova 513/22, 616 00 Brno, Czech Republic*
[2]*Brno University of Technology, Veveří 331/95, 602 00 Brno, Czech Republic*

Abstract

Our study utilizes a range of cumulative fatigue damage models to better understand the behavior of high-strength steels, addressing some of the shortcomings in current methodologies. To achieve this goal, a series of mechanical tests were performed on two types of HSS, S690, and S960, to understand the properties of these materials and determine their effect on the ability to resist fatigue damage. The accuracy of each model is determined based on the fatigue tested and S-N curves formed. The results are analyzed to determine which models are appropriate for predicting the fatigue behavior of high-strength steels. Overall, this study provides valuable insight into the fatigue behavior of HSS and highlights the need for further research in this area. By expanding our understanding of the properties of HSS, we can continue to develop new and innovative ways to utilize this material in construction, ultimately leading to safer and more reliable structures.

1. Introduction

The utilization of high-strength steel (HSS) in construction has become increasingly popular due to its remarkable properties. This type of steel is widely used for the construction of bridges, elements, and engineering parts due to its superior strength-to-weight ratio and cost efficiency [1]; the impressive strength-to-weight ratio of high-strength steels has led to their increased use in structural applications, though their fatigue resistance remains an area for further investigation [2].

However, an important factor that needs to be considered is the fatigue resistance of this material. Recent bridge construction has seen a significant increase in the use of high-strength steel for the primary structural elements [3].

A notable example of using HSS in bridge construction is the Akashi Kaikyō bridge in Japan. Grades S690 and S780 were used to construct this suspension bridge, one of the longest in the world. These HSS grades offer exceptional strength and durabil-

ity, making them ideal for large structures such as bridges [4].

In addition to the Akashi-Kaikyō bridge, HSS has also been used in various other bridge structures worldwide. For example, a hybrid girder bridge in Sweden, a composite bridge in Ingolstadt, Germany, and the roof truss of the Sony Center in Berlin are just a few examples of structures where S690 grade HSS has been used [2].

The use of HSS in bridge construction offers several advantages. First, it offers a high strength-to-weight ratio, which allows for lighter and more cost-effective structures. Second, HSS offers excellent durability and corrosion resistance, contributing to longer structural life. Finally, the esthetic appeal of HSS is another important factor contributing to its popularity in bridge construction [5].

Overall, the increasing use of HSS in bridge construction is a positive trend that has the potential to revolutionize the industry. With continued research and development in this area, we can expect to see even more innovative applications of HSS in the design

---

*Corresponding author: e-mail address: seitl@ipm.cz

Table 1. Chemical composition of S690 and S960, according to the producer list

S690		S960	
Chemical component	Percentage (%)	Chemical component	Percentage (%)
C	0.077	C	0.172
Si	0.391	Si	0.277
Mn	1.640	Mn	1.100
P	0.009	P	0.007
S	0.001	S	0.001
Al	0.094	Al-G	0.095
Cr	0.173	Cr	0.623
Ni	0.170	Ni	0.034
Mo	0.218	Mo	0.612
Cu	0.013	Cu	0.024
V	0.034	V	0.002
Nb	0.029	Nb	0.029
Ti	0.003	Ti	0.003
N	0.004	N	0.005
B	0.001	B-G	0.003
Zr	0.002	Zr	0.001
Ca0	0.450	Ca1	0.610

and construction of bridges and other large structures [6].

By studying steels S690 and S960, we can explore the fatigue behavior of HSS to better understand its potential benefits and how it responds to cyclic loading. To achieve this goal, the following methods were employed:

– Conducting a comprehensive review of existing literature on HSS [7].

– Determining several mechanical characteristics of selected HSS grades, including ultimate stress, yield stress, Young's modulus, and Vickers Pyramid Number (HV).

– Studying the theoretical framework of fatigue behavior under various stress levels.

– Determining the fatigue mechanical characteristic for uniaxial load S-N curve for stress ratio $R = 0.1$ using the Basquin model and under different load levels:

$$\sigma_{\mathrm{a}} = \sigma_{\mathrm{f}'} \left(2N_{\mathrm{f}}\right)^{b}, \qquad (1)$$

where σ_{a} is the stress amplitude, $\sigma_{\mathrm{f}'}$ is the fatigue strength coefficient, N_{f} is the number of cycles to failure, and b is the fatigue strength exponent.

– Analyzing the fatigue behavior of HSS under various stress levels and selecting the best criterion for HSS based on Palmgren-Miner's rule-based models:

$$D = \sum \left(N_i n_i\right), \qquad (2)$$

where D is the cumulative damage, n_i is the number of cycles at a given stress level, and N_i is the number of cycles to failure at the same stress level.

By utilizing these methods, the paper aims to provide valuable insights into the behavior of HSS in fatigue, which can help to optimize the design and construction of structures that utilize this material. The results of this research will also highlight the importance of considering fatigue resistance when working with HSS, especially in civil engineering applications where structures are subjected to cyclic loading. Overall, this study contributes to the expanding knowledge of HSS and its potential applications, ultimately leading to safer and more reliable structures.

2. Material tested

The chemical composition of both steel grades, S690 and S960, is specified in the EN-10025-6 standard (2004) and presented in Table 1.

3. Experimental results

An experimental program was performed on the two selected HSS, S690, and S960, by running the following tests: tensile test, Vickers hardness test and fatigue test. The results are presented in the following sections.

3.1. Tensile test

Results for the tensile test on S690 and S960 specimens are shown in Tables 2 and 3, respectively. This is followed by a representation of the stress-strain di-

T a b l e 2. S690 tensile test results

S690 No.	D_{o} (mm)	$\sigma_{\mathrm{y}}(Rp0.2)$ (MPa)	$\sigma_{\mathrm{u}}(Rm)$ (MPa)	A (%)
1	6.001	807.820	868.190	18.5
2	6.005	818.560	875.710	17.0
3	6.017	813.070	873.430	18.7
4	5.979	825.720	879.930	17.3
5	6.010	820.340	876.830	18.1
Average	6.002	817.102	874.818	17.9

T a b l e 3. S960 tensile test results

S960 No.	D_{o} (mm)	$\sigma_{\mathrm{y}}(Rp0.2)$ (MPa)	$\sigma_{\mathrm{u}}(Rm)$ (MPa)	A (%)
1	5.995	1,045.630	1,082.330	18.2
2	5.994	1,034.410	1,082.090	18.3
3	5.999	1,039.400	1,082.500	18.1
4	5.993	1,040.610	1,082.940	18.7
5	5.997	1,040.100	1,083.710	17.7
Average	5.996	1,040.300	1,082.714	18.2
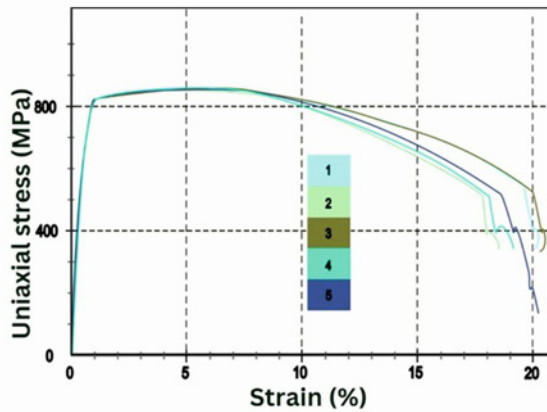
Fig. 1. Stress-strain diagram for S690 specimens.
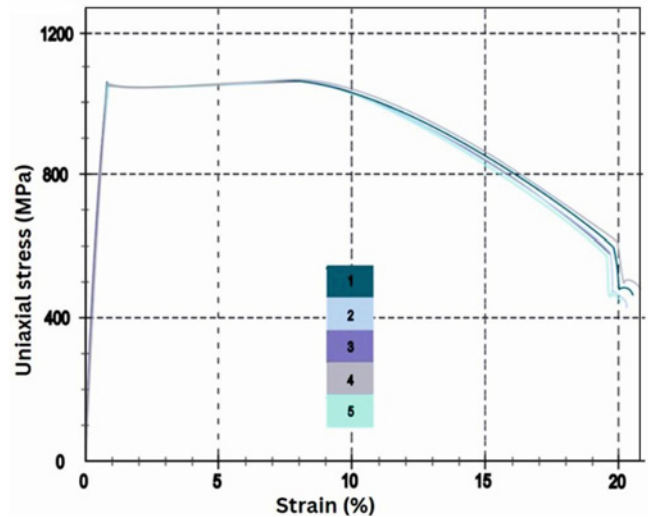
Fig. 2. Stress-strain diagram for S960 specimens.

agrams for the tested specimens, shown in Figs. 1, 2 in the same order [8].

These tensile test results, which were displayed, demonstrate that the behavior of the specimens was generally consistent with one another, with only a few minor variations in capacity and elongation (capacity ranging from 868.190 to 879.930 MPa and elongation between 17 and 18.7 % in the case of S690). Similarly, the S960 data showed almost no variation in capacity and elongations between 17.7 and 18.7 %.

3.2. Vickers hardness test

Standard metallographic techniques were used to prepare and polish the test specimens. The measurements were done in two different directions: vertically and horizontally, similarly to [9]. For S690 and S960,

respectively, Tables 4 and 5 summarize the results of the HV measurement. Moreover, red and blue colors, respectively, are used to indicate the values of the highest and minimum readings.

Regardings of the S690 hardness test in Table 4 showed that HV values for horizontal shifting resulted in smaller deviation (9.680) compared to vertical shifting (12.470), with minimum and maximum readings of 271–293 and 283–315, respectively.

The readings in Table 5 display the S960 hardness test results and show that horizontal shifting yielded a significantly lower deviation (0.632) than vertical shifting (8.710), with minimum and maximum readings of 355–357 and 336–356, respectively.

T a b l e 4. Vickers hardness test results for S690

S6 = S690 2 mm horizontal shift				S6 = S690 2 mm vertical shift			
#	D_1	D_2	HV	#	D_1	D_2	HV
1	80.680	81.250	283	1	80.470	81.040	284
2	81.220	80.120	285	2	77.330	76.040	315
3	82.140	83.330	271	3	79.630	79.710	292
4	81.720	83.540	272	4	80.680	81.250	283
5	80.680	78.540	293	5	80.470	78.330	294
6	79.840	79.170	293	6	81.930	80.210	282
Standard deviation			9.600	Standard deviation			12.400

T a b l e 5. Vickers hardness test results for S960

S6 = S960 2 mm horizontal shift				S6 = S960 2 mm vertical shift			
#	D_1	D_2	HV	#	D_1	D_2	HV
1	72.320	72.080	356	1	73.990	74.580	336
2	72.320	72.080	356	2	73.780	74.580	337
3	72.320	72.080	356	3	73.780	73.750	341
4	72.110	72.50	355	4	72.32	72.08	356
5	72.320	71.880	357	5	72.52	72.92	351
6	72.320	72.080	356	6	73.56	71.46	353
Standard deviation			0.630	Standard deviation			8.710

Fig. 3. The specimen used for fatigue testing.

3.3. Fatigue test

The prepared specimens are the same type as shown in Fig. 3. The specimens were positioned perpendicular to the rolling direction when we suspected the crack initiation. The specimens were tested for fatigue under the stress ratio $R = 0.1$ [10]. The S-N curves in Fig. 4 represent the results of the test. We can see that the S690 specimens are represented in circles (red: breaking, green: run out), and the S960 are in squares (yellow: breaking, blue: run out). The green mark refers to the specimens that reached the fatigue limit of 10^7 cycles, while the red mark means that the specimens broke before that.

The S-N curves indicate that most of the specimens in both HSS grades exhibit similar behavior, except for a few outliers on either side of the curve. These outliers include specimens that fracture at a low cycle count even under low-stress amplitudes or fail to complete the test under high-stress amplitudes. These outliers had a significant impact on the expected results of the experiment. Several factors, ranging from the steel's manufacturing process to its preparation in the lab to the testing of the specimens, may have contributed to these results. Therefore, additional testing should be conducted and monitored to identify the specific factors involved.

4. Cumulative fatigue damage models

Firstly, we performed further fatigue testing under various combinations of stresses for both S690 and S960 to be used in the models. In the case of S690 steel, three stress levels of 950, 975, and 990 MPa were selected and applied in a different order in each case

Fig. 4. *S-N* curves for S690 and S960 specimens under stress ratio $R = 0.1$.

Table 6. Stress combinations for S690

	Order	#	$\sigma_{\max}$ (MPa)	$N_{\mathrm{f}}(-)$
Case 1	1	A	950	100,000
	2	B	975	100,000
	3	C	990	61,700
Case 2	1	B	975	100,000
	2	A	950	100,000
	3	C	990	3,478,500
Case 3	1	C	990	100,000
	2	A	950	100,000
	3	B	975	10,000,000
Case 4	1	C	990	100,000
	2	B	975	100,000
	3	A	950	4,800
Case 5	1	B	975	100,000
	2	C	990	100,000
	3	A	950	10,000,000
Case 6	1	A	950	100,000
	2	C	990	100,000
	3	B	975	10,000,000

Table 7. Stress combinations for S960

	Order	#	$\sigma_{\max}$ (MPa)	$N_{\mathrm{f}}(-)$
Case 1	1	A	980	100,000
	2	B	1,000	95,200
	3	C	1,025	–
Case 2	1	B	1,000	100,000
	2	C	1,025	22,700
	3	A	980	–
Case 3	1	C	1,025	76,000
	2	A	980	–
	3	B	1,000	–

(see 6 various combinations altogether in Table 6). The specimens that did break are marked in red, while those that didn't are in green. Note that the stress levels during the cyclic loading were changed after reaching 100,000 cycles.

With regard to the S960 steel, the same concept was used with stress combinations of 980, 1000, and 1025 MPa at the start, but because the specimens broke in each of the first three cases, there was no need for further testing. Similar to Table 6, the red color in Table 7 represents the specimens that did break.

4.1. Palmgren-Miner model

Miner and Palmgren first proposed [11] the cumulative fatigue damage rule, commonly known as Miner's, to predict the failure of a component subjected to stresses of varying amplitude across a specific set of cycle blocks. It has been adopted in leading design standards for steel structures such as EN 1993-1-9:2005 [12] and DNVGL-RP-C203:2016 [13]. To calculate the total number of cycles based on Palmgren-Miner rule, we can see its representation in Eq. (3) below:

$$N_{\text{total}} = \frac{1}{\sum \dfrac{D_i f_i}{N_{\mathrm{f}_i}}}, \qquad (3)$$

T a b l e 8. Number of cycles extracted from S-N curves

S690				S960			
#	$\sigma_{\max}$(MPa)	N_i(−)	σ_{a}(MPa)	#	$\sigma_{\max}$ (MPa)	N_i(−)	σ_{a} (MPa)
1	950	57,500	427.5	1	980	124,500	441
2	975	42,200	438.6	2	1000	94,000	450
3	990	35,180	445.5	3	1025	66,700	461.3

where $D_i = n_i/N_{\mathrm{f}_i}$ is the damage at each stress level,

$$f_i = \frac{n_i}{\text{The total number of cycles}}$$

is the frequency of occurrence for each stress level, n_i is the number of cycles at each stress level from our experiment, and N_{f_i} is the number of cycles to failure at each stress level from the S-N curve [11].

Recognizing the limitations of the Palmgren-Miner rule, particularly its omission of stresses below the fatigue limit, we also evaluate the Haibach and Corten-Dolan models, which have been suggested to offer a more comprehensive approach to modeling fatigue damage under complex loading scenarios [14]. At the start of calculating the outcome of the models, we excluded the non-breaking specimens to achieve a steeper S-N curve with more reliable values, which is displayed in Table 8.

4.1.1. Steel S690

To calculate the damage caused by each stress level, we used the data in Tables 6–8 and based on Eq. (3).

Each set includes the number of cycles (n_i), number of cycles to failure (N_{f_i}), calculated damage (D_i), and frequency (f_i):

1. $n_1 = 57{,}500$, $N_{\mathrm{f}_1} = 100{,}000$, $D_1 = 0.575$, $f_1 = 0.4263$,

2. $n_2 = 42{,}200$, $N_{\mathrm{f}_2} = 100{,}000$, $D_2 = 0.422$, $f_2 = 0.3129$,

3. $n_3 = 35{,}180$, $N_{\mathrm{f}_3} = 61{,}700$, $D_3 = 0.5702$, $f_3 = 0.2607$.

The total number of cycles to failure for S690 is $N_{\mathrm{total,S690}} \approx 161{,}763$ cycles.

Therefore, if we use an Eq. (3) stress levels system of 427.5, 438.75, and 445.5 MPa with the given number of cycles, the theoretical results using Palmgren-Miner model predict that the total number of cycles to failure will be 161,763 cycles.

4.1.2. Steel S960

Similar to what we did with the S690 steel, we will calculate the damage caused by each stress level using the data in Tables 6–8 and based on Eq. (3).

Each set includes the number of cycles (n_i), number of cycles to failure (N_{f_i}), calculated damage (D_i), and frequency (f_i):

1. $n_1 = 124{,}500$, $N_{\mathrm{f}_1} = 100{,}000$, $D_1 = 1.245$, $f_1 = 0.4365$,

2. $n_2 = 94{,}500$, $N_{\mathrm{f}_2} = 95{,}200$, $D_2 = 0.987$, $f_2 = 0.3296$,

3. $n_3 = 66{,}700$, $N_{\mathrm{f}_3} = 100{,}000$, $D_3 = 0.667$, $f_3 = 0.2339$.

The total number of cycles to failure for S960 is $N_{\mathrm{total,S960}} \approx 96{,}031$ cycles.

Therefore, if we use an Eq. (3) stress levels system of 441, 450, and 461.25 MPa with the given number of cycles, the theoretical results using the Palmgren-Miner model predict that the total number of cycles to failure will be 96,031 cycles.

4.2. Haibach model

Under Haibach's proposal [15], the S-N curve would be extended from the knee point with a slope of $-1/(2m-1)$, which equals $2k-1$. The parameter m reflects the S-N curve's slope factor as $\sigma = bN - 1/m$.

4.2.1. Steel S690

Haibach's cumulative damage rule is displayed in the following Eq. (4):

$$\sum \frac{D_i}{N_i} = \left((\sigma - \sigma_{\mathrm{k}}) / (\sigma_{\mathrm{a}} - \sigma_{\mathrm{k}}) \right)^m, \qquad (4)$$

where D_i is the damage caused by the i-th stress level, N_i is the total number of cycles spent at the i-th stress level, σ is the stress level, σ_{k} is the knee point stress level, σ_{f} is the fatigue limit stress level, m is the material-specific constant, and $\sum$ is the summation over all stress levels.

To apply this model to our database and the given stress levels, we must first determine the knee point and the material-specific constant m. In our case, we will use the three-point method involving three selected points on the S-N curve: one at the high-stress end, one at the low-stress end, and one in the transition region. These points are used to determine the slope of the curve at each point, and the point where the slope changes from a relatively steep slope to a

much shallower slope is identified as the knee point [15].

Based on the available data, we can say that the knee point is at a stress level of 376 MPa.

Next, we can calculate the material-specific constant m. This can be done using the following Eq. (5):

$$m = \log\left(\frac{\sigma_f - \sigma_k}{\sigma_f - \sigma_i}\right) / \log\left(\frac{\sigma_f - \sigma_k}{\sigma_f - N}\right), \quad (5)$$

where σ_f is the fatigue limit stress level, which we will consider as 353 MPa.

In our cases, the knee point occurred at a higher stress level than the fatigue limit since the materials gradually transitioned from crack initiation to crack growth. This can happen, for example, if the material has a microstructure that allows it to sustain small cracks at higher stress levels before they grow and cause failure. In such cases, the S-N curve may have a long tail that extends beyond the fatigue limit, and the knee point may occur at a higher stress level. However, this is not the typical behavior for most engineering materials, and the knee point is usually located at a lower stress level than the fatigue limit [16].

Using the given equation for the S-N curve, we can solve it for σ and N as follows:

$$\sigma = 468.57 \times N^{-0.018},$$

$$N = (468.57/\sigma)^{(1/-0.018)}.$$

Substituting these values into Eq. (5) for m, we get:

$$m = \log\left(\frac{353 - 376}{353 - \dfrac{468.57^{-0.018}}{42,200}}\right) /$$

$$\log\left(\frac{353 - 376}{353 - \dfrac{468.57^{-0.018}}{438.75}}\right) = 8.695.$$

We can now use the given stress levels and number of cycles to calculate the damage caused by each stress level using the Haibach model:

For the first stress level (441 MPa): $D_1 = 0.1345$.
For the second stress level (450 MPa): $D_2 = 0.1107$.
For the third stress level (461.25 MPa): $D_3 = 0.0905$.

The total damage for all three stress levels applied consecutively is:

$$\sum(D_i) = 0.1345 + 0.1107 + 0.0905 = 0.3357.$$

Next, we can calculate the total number of cycles to reach failure as in Eq. (6):

$$N_t = 1/(D_1/n_1 + D_2/n_2 + D_3/n_3) =$$
$$1/(0.1345/57,500 + 0.1107/42,200 + 0.0905/3,518)$$
$$= 132,716.9 \text{ cycles.} \quad (6)$$

4.2.2. Steel S960

By following the same criteria we did in the S690 calculations, we do the same here (by using Eqs. (4)–(6)). And by having the values of the knee point equal to 392.44 MPa or taking it as 393 MPa and a fatigue limit stress level σ_f equals 378 MPa, we get:

Using the given equation for the $S - N$ curve, we can solve for σ and N as follows:

$$\sigma = 630.27 \times N^{-0.032},$$

$$N = (630.27/\sigma)^{(1/-0.032)}.$$

Substituting these values into the equation for m (according to the Eq. (5)), we get:

$$m = \log\left(\frac{378 - 393}{378 - \dfrac{630.27^{-0.032}}{112,200}}\right) /$$

$$\log\left(\frac{378 - 393}{378 - \dfrac{630.27^{-0.032}}{441}}\right) = 9.373.$$

We can now use the given stress levels and number of cycles to calculate the damage caused by each stress level using Haibach model:

For the first stress level (441 MPa): $D_1 = 0.0708$.
For the second stress level (450 MPa): $D_2 = 0.1837$.
For the third stress level (461.25 MPa): $D_3 = 0.4736$.

The total damage for all three stress levels applied consecutively is:

$$S(D_i) = 0.0708 + 0.1837 + 0.4736 = 0.7281.$$

Next, we can calculate the total number of cycles to reach failure as follows:

$$N_t = 1/(D_1/n_1 + D_2/n_2 + D_3/n_3) =$$
$$1/(0.0708/124,500 + 0.1837/9,400 + 0.4736/66,700)$$
$$= 103,913.59 \text{ cycles.}$$

4.3. Corten-Dolan model

According to Corten & Dolan [17], their model is an extension of Miner's rule and considers the effects of different stress levels on fatigue damage. The model assumes that the fatigue damage accumulated under

different stress levels can be linearly superimposed to obtain the total fatigue damage. The equation for the Corten-Dolan model is:

$$D_{cr} = p_{max} r_{max} N_{f_{max}}^{a_{max}}, \tag{7}$$

where a_{max}, p_{max}, and r_{max} represent the material constant, the number of damaged nuclei, and the damage coefficient due to the maximum stress level σ_{max}, respectively. The fatigue life at the maximal stress level is known as $N_{f_{max}}$ [17].

The cumulative damage of the specimen under multi-level variable amplitude loading can be determined by adding the damage sustained under the combined action of all loading levels and by adding the cumulative damage D corresponding to the loading until the failure is equal to the critical damage D_c [13]. The following formula in Eq. (8) can be used to describe the cumulative damage of the specimen under the changing amplitude load of n:

$$D = \sum_{i=1}^{n} p_i r_i n_i^{a_i} = p_{max} r_{max} N_{f_{max}}^{a_{max}}. \tag{8}$$

Corten & Dolan [17] examined a substantial amount of test data and proposed two hypotheses: The first assumption is that the number of damaged cores in the loading process is dependent on the high degree of stress, and once formed, it will continue to build up until failure, therefore $p_i = p_{max}$. The second assumption is that $(r_i/r_{max})^{1/a} = (\sigma_i/\sigma_{max})^d$ and that $a = a_i = a_{max}$. The fatigue life prediction format of the Corten-Dolan model under multistage variable amplitude loading can be expressed as follows using Eq. (9) and the above two assumptions:

$$N_{CD} = \frac{N_{f_{max}}}{\sum_{i=1}^{n} a_i (\sigma_i/\sigma_{max})^d}, \tag{9}$$

where a_i is the ratio of the number of cycles corresponding to the i-th stress level to the total number of cycles, and N_f is the fatigue life predicted by the Corten-Dolan model under cyclic loading of level n. The material constant is d; it can range from 4.8 for high-strength steels to 5.8 for other materials [17].

4.3.1. Steel S690

First, we need to calculate the damage ratio and slope for each stress level using the S-N curve equation and the fatigue limit of the material:

For the first stress level (427.5 MPa):
$r_1 = 353/427.5 = 0.8257$,
$a_1 = -0.018$.
For the second stress level (438.75 MPa):

$r_2 = 353/438.78 = 0.8046$,
$a_2 = -0.018$.
For the third stress level (445.5 MPa):
$r_3 = 353/445.5 = 0.7924$,
$a_3 = -0.018$.

Next, we can calculate the probability of each stress level occurring:
$$p_i = (\sigma_a - \sigma_{min})/(\sigma_{max} - \sigma_{min}),$$
$$p_1 = (427.5 - 95)/(950 - 95) = 0.3782,$$
$$p_2 = (450 - 100)/(1000 - 100) = 0.3648,$$
$$p_3 = (461.25 - 102.5)/(1025 - 102.5) = 0.2570.$$
The probability of the maximum stress level occurring is $p_{max} = p_3 = 0.2570$.

Using the given number of cycles, we can calculate the total fatigue damage caused by each stress level:
For the first stress level (427.5 MPa):

$$D_1 = p_1 \times r_1 \times n_1^{a_1} = 0.3782 \times 0.8257 \times 20{,}000^{-0.018}$$
$$= 0.2613.$$

For the second stress level (438.75 MPa):

$$D_2 = p_2 \times r_2 \times n_2^{a_2} = 0.3648 \times 0.8046 \times 20{,}000^{-0.018}$$
$$= 0.2456.$$

For the third stress level (445.5 MPa):

$$D_3 = p_3 \times r_3 \times n_3^{a_3} = 0.2570 \times 0.7924 \times 20{,}000^{-0.018}$$
$$= 0.1704.$$

Finally, we can use the Corten-Dolan model equation to calculate the total fatigue damage caused by the three stress levels:

$$\sum D = 0.2613 + 0.2456 + 0.1704 = 0.6773.$$

Therefore, the total fatigue damage caused by the three stress levels is 0.6773.

We can also use the Corten-Dolan model to estimate the number of cycles to failure based on the total fatigue damage. Using Eq. (9) and assuming $d = 4.8$ for HSS, we get:

$$D_{CD} = 266{,}000/\left(0.1747 \times \left(\frac{427.5}{445.5}\right)^{-4.8} + \right.$$
$$\left. 0.7354 \times \left(\frac{438.75}{445.5}\right)^{-4.8} + 1.0 \times \left(\frac{445.5}{445.5}\right)^{-4.8}\right),$$
$$D_{CD} = 132{,}717.2 \text{ cycles.}$$

4.3.2. Steel S960

The same procedure was applied to S690. First, we need to calculate the damage ratio and slope for each stress level using the S-N curve equation and the fatigue limit of the material:

For the first stress level (441 MPa):
$r_1 = 378/441 = 0.8571$,
$a_1 = -0.032$.
For the second stress level (450 MPa):
$r_2 = 378/450 = 0.8400$,
$a_2 = -0.032$.
For the third stress level (461.25 MPa):
$r_3 = 378/461.25 = 0.8195$,
$a_3 = -0.032$.

Next, we can calculate the probability of each stress level occurring:
$$p_i = (\sigma_a - \sigma_{min})/(\sigma_{max} - \sigma_{min}),$$
$$p_1 = (441 - 98)/(980 - 98) = 0.3989,$$
$$p_2 = (450 - 100)/(1000 - 100) = 0.3846,$$
$$p_3 = (461.25 - 102.5)/(1025 - 102.5) = 0.2165.$$

The probability of the maximum stress level occurring is $p_{max} = p_3 = 0.2165$.

Using the given number of cycles, we can calculate the total fatigue damage caused by each stress level.

For the first stress level (441 MPa):

$$D_1 = p_1 \times r_1 \times n_1^{a_1} =$$
$$0.3989 \times 1.0884 \times 100,000^{-0.032} = 0.3004.$$

For the second stress level (450 MPa):

$$D_2 = p_2 \times r_2 \times n_2^{a_2} =$$
$$0.3846 \times 1.0667 \times 100,000^{-0.032} = 0.2838.$$

For the third stress level (461.25 MPa):

$$D_3 = p_3 \times r_3 \times n_3^{a_3} =$$
$$0.2165 \times 1.0391 \times 100,000^{-0.032} = 0.1556.$$

Finally, we can use the Corten-Dolan model equation to calculate the total fatigue damage caused by the three stress levels:

$$\sum D = 0.3004 + 0.2838 + 0.1556 = 0.7398.$$

Therefore, the total fatigue damage caused by the three stress levels is 0.7398.

We can also use the Corten-Dolan model to estimate the number of cycles to failure based on the total fatigue damage. Using Eq. (9) and assuming $d = 4.8$ for HSS, we get:

$$D_{CD} = 153386 / \left(0.2165 \times \left(\frac{441}{461.25} \right)^{-4.8} + \right.$$
$$\left. 1.0884 \times \left(\frac{450}{461.25} \right)^{-4.8} + 1.0391 \times \left(\frac{461.25}{461.25} \right)^{-4.8} \right),$$
$$D_{CD} = 60,554.5 \text{ cycles.}$$
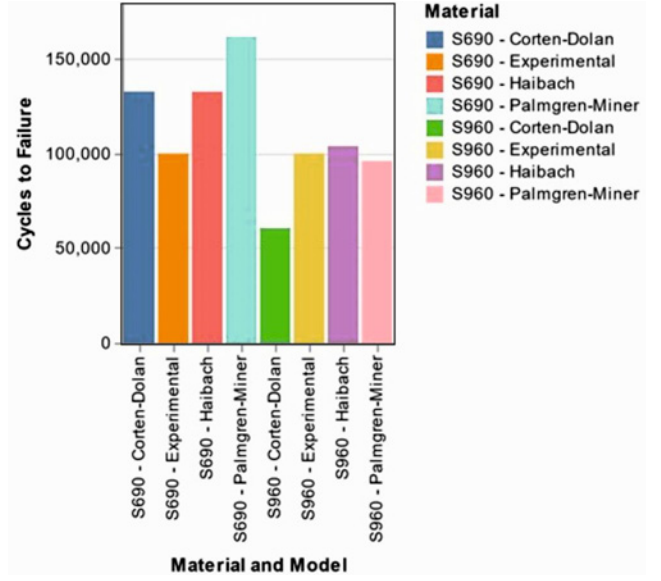
Fig. 5. Bar-chart diagram illustrating the comparative analysis of life cycles for S690 and S960, comparing experimental data with predictions from the Palmgren-Miner, Haibach, and Corten-Dolan models.

5. Evaluation and discussion

In our study, we tested two high-strength steels, S690 and S960, and compared the predictions of three commonly used fatigue models: Palmgren-Miner, Haibach, and Corten-Dolan. We evaluated the performance of each model by comparing their predictions with the actual experimental results obtained from testing six specimens of each material.

The experimental variability observed in our results echoes the complexities identified in modeling fatigue life under non-Gaussian random loading, underscoring the need for robust and versatile fatigue models that can accommodate such discrepancies [18].

For S690, the Palmgren-Miner model predicted the total number of cycles to failure of 161,763, while the Haibach model predicted the total number of cycles to failure of 132,717. The Corten-Dolan model predicted the total number of cycles to failure of 132,717.

The experimental results (see Table 6) show significant variation in the number of cycles to failure for each specimen, ranging from 4,800 cycles to 10,000,000 cycles. However, the predicted values from all three models fall within the range of the experimental results. The original model is the closest in terms of total damage and number of cycles to failure, with predicted values that are slightly higher than the other results. The Haibach model is also fairly accurate along with the Corten-Dolan model, but it predicts a slightly shorter fatigue life than the experimental results.

For S960, the Palmgren-Miner model predicted the total number of cycles to failure of 96,031, while the

Haibach model predicted the total number of cycles to failure of 103,913. The Corten-Dolan model predicted the total number of cycles to failure of 60,555.

In this case, the experimental results show a shorter fatigue life for S960 than for S690. This is likely due to the fact that we have used higher stress levels when testing for the S960 because it's more resistant to fatigue failure. However, the predicted values from all three models fall within the range of the experimental results. The Haibach model is the closest in terms of total damage and number of cycles to failure, with predicted values that are only slightly higher than the results of the other models. The Corten-Dolan model predicts a significantly shorter fatigue life, while the Palmgren-Miner model is closer to the Haibach model.

Overall, our study suggests that the choice of fatigue model can significantly impact the accuracy of predictions for high-strength steels. The original model is the most accurate for predicting fatigue life in S690, while the Haibach model is the most accurate for predicting fatigue life in S960. However, it is important to note that all three models provide reasonably accurate predictions for both materials.

It is also worth noting that other factors can affect the accuracy of fatigue life predictions for high-strength steels, such as the presence of defects or the effect of mean stress on fatigue life. Therefore, it is important to use multiple models and validate their predictions using experimental data in order to ensure accurate and reliable fatigue life predictions.

Based on the analysis and comparison of the fatigue models, it is clear that each model has its own strengths and weaknesses when applied to the high-strength steel specimens of S690 and S960 MPa. The Palmgren-Miner model, despite its simplicity, provides a reasonable estimate of the total damage and number of cycles to failure for both the S690 and S960 MPa specimens. The Haibach model, on the other hand, provides a more accurate prediction for the S960 MPa specimen but is less accurate for the S690 MPa specimen. Finally, while the Corten-Dolan model provides a relatively accurate prediction of the total number of cycles to failure for both specimens, it overestimates the total damage for both the S690 and S960 MPa specimens.

Therefore, when choosing a fatigue model for high-strength steel specimens, it is important to consider the intended application and level of accuracy required. In cases where a quick estimate is required, the Palmgren-Miner model may suffice, while the Haibach model may be more appropriate for more critical applications requiring higher accuracy. However, it is important to note that no model is perfect, and experimental validation is always recommended to ensure the accuracy and reliability of the results.

In terms of further research, exploring other fatigue models and comparing their performance to the models used in this study may be beneficial. Additionally, it may be useful to investigate the effects of different factors, such as loading conditions and specimen geometries, on the performance of the fatigue models. Finally, conducting more experimental tests on a larger sample size and a wider range of loading conditions may provide more comprehensive data for future research and development in fatigue analysis.

6. Conclusions

Our findings, which reveal a significant impact of model selection on predictive accuracy, resonate with the broader academic discourse on fatigue modeling. The work serves as a touchstone for our study, reinforcing the importance of careful model choice in predicting the fatigue life of high-strength steels [1].

Two high-strength steels, S690 and S960, were tested to obtain their basic mechanical and fatigue properties. Furthermore, predictions of the total damage and number of cycles to failure were performed by means of three commonly used fatigue models: Palmgren-Miner, Haibach, and Corten-Dolan. The performance of each model was evaluated by comparing the results with the actual experimental results obtained from testing six specimens of each material (considering three stress levels for each specimen). It has been shown that the choice of the fatigue model can significantly impact the accuracy of predictions for high-strength steels. Thus, it is important to consider the intended application and level of accuracy required (in cases where a quick estimate is required, the Palmgren-Miner model may be sufficient, while the Haibach model may be more appropriate for more critical applications requiring higher accuracy). However, no model is perfect, and experimental validation is recommended to ensure the reliability of the results.

References

[1] H. Gao, H. Z. Huang, Z. Lv, F. J. Zuo, H. K. Wang, An improved Corten-Dolan's model based on

damage and stress state effects, Journal of Mechanical Science and Technology 29 (2015) 3215–3223. https://doi.org/10.1007/s12206-015-0721-x

[2] C. M. Sonsino, T. Łagoda, G. Demofonti, Damage accumulation under variable amplitude loading of welded medium- and high-strength steels, International Journal of Fatigue 26 (2004) 487–495. https://doi.org/10.1016/j.ijfatigue.2003.10.001

[3] C. Huating, G. Grondin, R. Driver, Fatigue resistance of high performance steel, Structural Engineering Report 258, 2005. https://doi.org/10.7939/R31R6N19P

[4] Akashi Kaikyo Bridge, https://www.ice.org.uk/what-is-civil-engineering/ what-do-civil-engineers-do/akashi-kaikyo-bridge

[5] R. Bjorhovde, Development and use of high performance steel, Journal of Constructional Steel Research 60 (2004) 393–400. https://doi.org/10.1016/S0143-974X(03)00118-4

[6] C. Miki, K. Homma, T. Tominaga, High strength and high performance steels and their use in bridge structures, Journal of Constructional Steel Research 58 (2002) 3–20. https://doi.org/10.1016/S0143-974X(01)00028-1

[7] K. Hectors, W. De Waele, Cumulative damage and life prediction models for high-cycle fatigue of metals: A review, Metals 11 (2021) 204. https://doi.org/10.3390/met11020204

[8] ASTM, ASTM E8/E8M − 13-Standard Test Methods for Tension Testing of Metallic Materials.

[9] J. Klusák, V. Horník, G. Lesiuk, S. Seitl, Comparison of high- and low-frequency fatigue properties of structural steels S355J0 and S355J, Fatigue and Fracture of Engineering Materials and Structures 44 (2021) 3202–3213. https://doi.org/10.1111/ffe.13580

[10] ASTM, E140-05e1 – Standard Hardness Conversion Tables for Metals Relationship Among Brinell Hardness, Vickers Hardness, Rockwell Hardness, Superficial Hardness, Knoop Hardness, and Scleroscope Hardness.

[11] ASTM, E466-15 – Standard Practice for Conducting Force Controlled Constant Amplitude Axial Fatigue Tests of Metallic Materials.

[12] M. Miner, Cumulative damage in fatigue, Journal of Applied Mechanics 12 (1945) A159–A164. https://doi.org/10.1115/1.4009458

[13] SS-EN 1993-1-1:2005, Eurocode 3: Design Of Steel Structures – Part 1-1: General Rules And Rules For Buildings.

[14] DNVGL, RP-C203, Fatigue design of offshore steel structures. Technical Report, 2005

[15] E., Bohm, M. Kurek, T. Lagoda, Fatigue Damage Accumulation model of 6082-T6 aluminum alloy in conditions of block bending and torsion, Journal of Testing and Evaluation 48 (2020) 4416–4434. https://doi.org/10.1520/JTE20170598

[16] E. Haibach, Modified linear damage accumulation hypothesis accounting for a decreasing fatigue strength during increasing fatigue damage, Darmstadt: Laboratorium für Betriebsfestigkeit, LBF, TM Nr. 50, 1970.

[17] S. Schoenborn, H. Kaufmann, C. Sonsino, R. Heim, Cumulative damage of high-strength cast iron alloys for automotive applications, Procedia Engineering C 101 (2015) 440–449. https://doi.org/10.1016/j.proeng.2015.02.053

[18] A. Banvillet, T. Łagoda, E. Macha, A. Niesłony, T. Palin-Luc, J.-F. Vittori, Fatigue life under non-Gaussian random loading from various models, International Journal of Fatigue, 26 (2004) 349–363. https://doi.org/10.1016/j.ijfatigue.2003.08.017

[19] Z. Kala, Estimating probability of fatigue failure of steel structures, Acta et Commentatones Universitatis Tertuensis de Mathematica 23 (2019) 245–254. https://doi.org/10.12697/ACUTM.2019.23.21

[20] R. C. Hibbeler, Mechanics of Materials, 11th Edition, Pearson 2022. ISBN-10: 0137605587